19th Brazilian Congress of Thermal Sciences and Engineering
November 06th-10th, 2022, Bento Gonçalves - RS - Brazil

ENC-2022-0094
A PURELY LAGRANGIAN METHOD FOR SIMULATING SURFACE ROUGHNESS EFFECTS ON FLOW PAST A SOLID BODY

Fabio Eduardo Ferraz de Carvalho
School of Engineering, São Paulo State University (UNESP), Guaratinguetá SP 12.516-410, Brazil
fabio.eduardo@unesp.br

Marcos André de Oliveira
Civil Engineering Department, Federal University of Tocantins (UFT), Palmas TO 77.001-090, Brazil
marcos.oliveira@uft.edu.br

Luiz Antonio Alcântara Pereira
Mechanical Engineering Institute, Federal University of Itajubá (UNIFEI), Itajubá MG 37.500-903, Brazil
luizantp@unifei.edu.br

Alex Mendonça Bimbato
School of Engineering, São Paulo State University (UNESP), Guaratinguetá SP 12.516-410, Brazil
alex.bimbato@unesp.br

Abstract. *Roughness is a key parameter in fluid-structure interaction problems. Several studies link roughness with variations in aerodynamic loads, turbulence transition, and in heat transfer. Recent studies have applied a Lagrangian vortex method associated with Large Eddy Simulation (LES) to examine the roughness influence on bluff body aerodynamics. In these works, the body surface is discretized through the panel method, in which the solid boundary is approximated to panels, over which constant-density sources are distributed. The present paper examines the possibility of using vortex distributions of linear density as the singularity of the panel method, making it possible to simulate rough slender bodies in addition to rough bluff bodies. In the present work, turbulence is modeled by a LES simulation adapted to the Lagrangian vortex method to simulate the two-dimensional turbulent flow past a circular cylinder that is disturbed by surface roughness effects. Different simulations are conducted at upper-subcritical Reynolds number flows of* $Re = 1.0 \times 10^5$*. When the roughness is considered, the simulations were able to correctly represent the delay in the boundary layer separation and the drop in drag coefficient due to the roughness effect. The results indicate that the use of a vortex distribution of linear density in the panel method can capture important turbulent flow characteristics and, as consequence, it can be used to simulate airfoils with rough surfaces.*

Keywords: *Lagrangian vortex method, roughness model, aerodynamic, panel method*

1. INTRODUCTION

A perfectly smooth surface is an idealization; in practical situations, any object has a rough surface. In fluid-structure interaction (FSI) problems, the ideally smooth surface hypothesis is acceptable when roughness dimensions are much smaller than the boundary-layer thickness (Chung et al., 2021). However, in many cases, the operational wear (Dalili et al., 2009), the action of external agents, such as solid particulars collision (Fiore & Selig, 2015), marine organisms' encrustation (Han et al. 2021), and surface icing (Toba et al., 2020), and even the manufacturing process (Pour, 2018), result in surfaces deformations, making the roughness effect not negligible. In these situations, the layers of fluid closest to the solid are disturbed by the rough surface topography, creating instabilities on the flow boundary layer. These instabilities anticipate the appearance of phenomena that would only occur at higher Reynolds numbers on flow over smooth surfaces.

In a flow around a solid, changes in directions are imposed on the flow by the impenetrability condition of the solid surface; this imposition creates an adverse pressure gradient. In viscous flows, the no-slip condition imposes zero relative velocity at the fluid layer near the surface of the solid. The small velocities and the adverse pressure gradient, near the solid surface, may result in the boundary layer separation. At the separation point, a flow in the opposite direction is established and the discontinuity between the main flow and that of the opposite direction leads to vortex formation. These vortices are shed into the flow and undergo melting, dilution, and stretching, thus forming the vortex wake downstream of the solid.

The vortex wake behavior changes with the Reynolds number. Williamson (1996) studied, experimentally, the flow around a hydraulically smooth cylinder and observed that among Reynolds numbers of 1.0×10^3 to 1.0×10^5, with the Reynolds number augmentation, the pressure coefficient at the back of the cylinder (base pressure coefficient) decreases, the Strouhal number ($St = f\,D/\,U$, where D is diameter and U is flow velocity) stay constant around 0.20 and the formation length of the mean recirculation region decreases, thus resulting in a narrow and shorter vortex formation region. Above Reynolds number of 1.0×10^5, at critical values of Reynolds, the author noted that the base pressure coefficient increases with the Reynolds augmentation, and a separation-reattachment bubble was formed on one side of the cylinder. At supercritical Reynolds numbers, the author registered the formation of the second separation-reattachment bubble, on the other side of the cylinder, and, as consequence, a higher Strouhal number is detected with a thinner vortex wake. This dependence of the vortex wake phenomena on Reynolds numbers has been registered by several papers (Achenbach & Heinecke, 1981; Han et al., 2021; Henderson, 1995; Norberg, 1994; Roshko, 1993; Slaouti & Gerrard, 1981; Unal & Rockwell, 1988; Williamson, 1996).

The roughness effect modifies the well-registered dependence of vortex wake phenomena and Reynolds numbers. Several works noticed that the presence of surface roughness provoked an early transition of the boundary layer and phenomena typical of high-Reynolds number flows occur at physically low Reynolds numbers, and as consequence, the fluid dynamic loads are disturbed. The experimental analysis conducted by van Hinsberg (2015) showed that at Reynolds numbers of $Re \sim 1.6 \times 10^5$, the drag coefficient values of a cylinder with a small surface roughness ($\varepsilon^*/D^* \sim 1.2 \times 10^{-3}$, where ε^*/D^* is the mean relative surface roughness) drop radically from ~1.2 to ~0.4. At a smooth cylinder ($\varepsilon^*/D^* \sim 1 \times 10^{-5}$), Schewe (1983) observed that the drag coefficient crisis happens only at Reynolds numbers of $Re \sim 2.6 \times 10^5$. With a large roughness ($\varepsilon^*/D^* \sim 30 \times 10^{-3}$), in a wind tunnel experiment of a flow around a cylinder, Achenbach & Heinecke (1981) registered the drag crisis at values of Reynolds number even lower ($Re \sim 2.0 \times 10^4$) than those of van Hinsberg (2015). At slender bodies, such as airfoils, the surface roughness affects the lift generation. Chakroun et al (2004) investigation of the effect of roughness at NACA0012 showed that the maximum lift coefficient of 0.9315 occurs at the attack's angle of α=10º for a smooth airfoil; when a roughness airfoil is tested, the maximum lift coefficient reached the value of 0.9626 at attack's angle of α=14º.

The modifications of the fluid dynamics load on flows around rough solid bodies are related to many issues and opportunities for engineering applications. Dalili et al. (2009) found that the increasement in surface roughness on the blades of a wind turbine due to the accumulation of insects may result in performance losses that can reach 50% in more severe cases. The work of Han et al. (2021) on the deposition of organisms in marine risers showed that as the surface roughness is altered by the accumulation of organisms, the response of the structure to the flow becomes more chaotic, increasing the frequency of excitation and reducing the structure useful life. On the other hand, the work of Kodancha & Salunkhe (2021) showed that it is possible to use the surface roughness at the leading edge of the blades of an axial compressor to control the leakage flow at the edges (Tip Leakage Flow – details in Zhang et al. (2021)) and increase the machine performance. The work of Wang et al. (2021) showed how the addition of surface roughness, in a controlled manner, can reduce the pressure on the roof of high-speed trains and control the stresses suffered by the structure due to gusts of wind. A better understanding of how roughness surface disturbs the flow dynamics can help manage the issues and seize the opportunities of roughness effects.

An important characteristic of the experimental studies with roughness effect is the difficulty of comparing results from different works. Data from experiments with the same Reynolds number and with the same relative roughness are very scatter, as register by Güven et al. (1980). The complexity to reproduce the same roughness surface topography, the blockage effect and perturbations on free-stream turbulence are main reasons to scatter results from experimental works (1998). Although some techniques to blockage correction are available in the literature and many works studied how to compare two roughness surface topographies by their equivalent sand-grain roughness (Adams et al., 2012), to compare data from different experimental studies of roughness effect is still a challenging task.

On the other hand, the numerical studies of flow around a rough body are still limited to low Reynolds numbers (van Hinsberg, 2015), and numerical data of aerodynamic loads for the flow past a rough cylinder at upper subcritical Reynolds number of $Re = 5 \times 10^4$ are very rare (Bimbato et al., 2020). At low Reynolds numbers, the Reynolds-Averaged Navier–Stokes (RANS) simulations are applied in an Eurelian schema with the shear stress transport (SST) k−ω turbulence model to analyze the flow around rough cylinders (Chen et al., 2022; Gao et al., 2018) At high

Reynolds numbers, recent studies have been successful in applying a Lagrangian vortex method associated with Large Eddy Simulation (LES) to examine the roughness influence on bluff body aerodynamics.

Bimbato et al. (2019) developed a two-dimensional roughness model based on a LES turbulence model proposed by Lesieur & Metais (1996) and adapted by Alcântara Pereira et al. (2003) to the two-dimension Lagrangian vortex method. The main strategy of the roughness model is to inject momentum into the flow boundary layer, stimulating turbulence and simulating the roughness effect. The most important features of the Lagrangian vortex method, namely being a free mesh technique and having the computational efforts concentrated on the regions of vorticity, are preserved by the proposed roughness model. In Oliveira et al. (2020) the roughness model was used to simulate the flow around a rough cylinder near a moving wall at Reynolds number of 1×10^5; the model was capable of correctly representing the drag reduction and the complete vortex shedding suppression due to rough effects and the moving ground proximity. Bimbato et al. (2020) were able to capture the bubble formation anticipation to subcritical Reynolds number flow due to the roughness effect, using the same roughness model at $Re = 1 \times 10^5$.

The works discussed in the previous paragraph employed the roughness model developed by Bimbato et al. (2019) in Lagrangian vortex methods simulations. In these simulations, the body surface is discretized through the panel method (Katz & Plotkin, 2001), in which the solid boundary is approximated to panels, over which singularities are distributed. The intensity of which singularity is calculated to enforce the impermeability boundary condition on the center of the panels. All the above-discussed papers applied the same type of singularity: the constant-density sources. Although this type of singularity is very common in vortex methods simulations, with numerical convergence and stability well documented, its use is restricted to simulations in which flow past over symmetrical bodies, where liftin is not expected. For non-symmetrical bodies, for instance, the airfoil with a non-zero attack angle, antisymmetric singularities such as the doublet or vortex should be used (Katz & Plotkin, 2001).

The present paper examines the possibility of using a vortex distribution of linear density as the singularity of the panel method in simulations with the roughness model developed by Bimbato et al. (2019). The discretization through flat panels with vortex distribution differs from source distribution making it possible to simulate slender bodies in addition to bluff bodies. Furthermore, the vortex distribution of linear density is of a higher order than the constant-density source distributions. The adaptations to the formulation of the panel method coupled with the vortex method, to consider the linear-density vortex distribution singularities, are discussed in section 2, together with a summary of the roughness model formulation. The results of three different simulations are presented and discussed in section 3: the laminar flow at Re = 1.0×10^5 past a smooth circular cylinder, the turbulent flow at Re = 1.0×10^5 past the same smooth cylinder; and lastly, the same turbulent flow around a rough ($\varepsilon^*/D^* = 0.007$) circular cylinder.

2. FORMULATION AND METHODS

2.1. Problem formulation and governing equations

The computational domain is described in a fixed Cartesian coordinate system (x^*, y^*). The x-axis is along the streamwise mean flow direction and the x^*-axis is perpendicular to the y^*-axis; the origin of the coordinate system is shown in Fig. 1. The circular cylinder is immersed in an infinity fluid domain, Ω. The symbol * is used to identify dimensional quantities; the D^* is the outer cylinder diameter, U^* is the incompressible inlet flow, and x^* and y^* are the global coordinate system. The fluid is Newtonian with constant kinematic viscosity, ν. The flow is assumed to be unsteady, incompressible, and two-dimensional. The surface S_b is the body surface, in which the impermeability and non-slip condition is enforced and the S_∞ is the boundaries far from the body, where the inlet flow is retrieved.

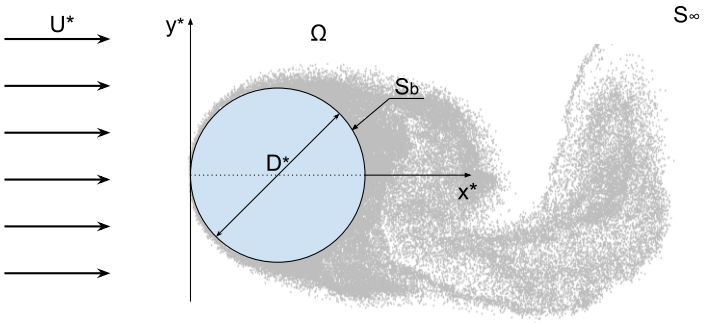

Figure 1. Definition of the fluid domain.

The problem governing equations are the continuity, Eq. (1), and the filtered Navier-Stokes (N-S), Eq. (2). The Eq. (2) is obtained through a LES modeling of the N-S equation, in which the large eddies are simulated, and the smaller ones are modeled. Applying a low-pass spatial filter to the N-S equations, the following equations for the filtered quantities written in Cartesian form, are obtained (Liang & Papadakis, 2007):

$$\frac{\partial \bar{u}_i^*}{\partial x_i^*} = 0 \tag{1}$$

$$\frac{\partial \bar{u}_i^*}{\partial t} + \frac{\partial}{\partial x_i^*}\left(\bar{u}_i^* \bar{u}_j^*\right) = -\frac{1}{\rho}\frac{\partial \bar{p}^*}{\partial x_i^*} + 2\frac{\partial}{\partial x_j^*}\left[(\nu + \nu_t)\bar{S}_{ij}^*\right] \tag{2}$$

Where the index $(i = 1,2)$ indicate the directions in the cartesian coordinate system, the $\bar{u}^*$ and the $\bar{p}^*$ terms are the filtered velocity and pressure, respectively; ν_t defines the local eddy viscosity coefficient and $\bar{S}_{ij}^*$ characterizes the deformation tensor of the filtered field. The $\bar{S}_{ij}^*$ term is calculated as presented by Smagorinsky (1963):

$$\bar{S}_{ij}^* = \frac{1}{2}\left(\frac{\partial \bar{u}_i^*}{\partial x_j^*} + \frac{\partial \bar{u}_j^*}{\partial x_i^*}\right) \tag{3}$$

According to Lesieur & Metais (1996), the local eddy viscosity coefficient at a point x^* in the flow field, and at an instant t^*, can be calculated via the local kinetic energy spectrum, Eq. (4):

$$\nu_t(x^*, \Delta^{+*}, t^*) = 0.105 C_k^{-3/2} \Delta^{+*} \sqrt{\overline{F_2^*}(x^*, \Delta^{+*}, t^*)} \tag{4}$$

Where the term C_k is the constant of Kolmogorov and has the value of 1.4, Δ^{+*} is the characteristic length scale and $\overline{F_2^*}(x^*, \Delta^{+*}, t^*)$ is the local second-order velocity structure function of the filtered field defined as follows:

$$\overline{F_2^*}(\boldsymbol{x}^*, \Delta^{+*}, t^*) = \left\| \overline{\overline{\boldsymbol{u}^*}(\boldsymbol{x}^*, t^*) - \overline{\boldsymbol{u}^*}(\boldsymbol{x}^* + \boldsymbol{r}^*, t^*)} \right\|^2_{\|\boldsymbol{r}^*\| = \Delta^{+*}} \tag{5}$$

The two governing equations, Eq. (1) and Eq (2), are numerically solved at fluid domain Ω (Fig. 1) and limited by three boundary conditions: no relative velocity between the solid and the fluid at the solid surface S_b in the direction normal to the surface (impermeability condition), no relative velocity between the solid and the fluid at the solid surface S_b in the direction tangential to the surface (no slip condition) and the free-stream velocity far away from the body at S_∞. The impermeability boundary condition is implemented through the panel method at which the solid surface is discretized in flat panels (Katz & Plotkin, 2001). The non-slip condition is assured through new vortex's generation and shedding in the fluid domain: the new vortices intensities are calculated such that the fluid velocity tangent to panel direction be zero at the panel center (Lewis, 1991). The faraway boundary condition is automatically satisfied due to Lagrangian vortex method formulation.

2.2. The Lagrangian vortex method with LES modeling

A Lagrangian discretization of the flow vorticity field is possible through the vortex method. The vorticity field ω is numerically approximated to $\bar{\omega}$ by NV vortex bubbles of radius $\sigma_0 = 1.41421\sqrt{\Delta t/Re}$, in which each discrete vortex element carries a constant circulation Γ_k (Lewis, 1991):

$$\bar{\omega}(\boldsymbol{x}, t) = \sum_{k=1}^{NV} \frac{\Gamma_k}{\pi \sigma_{0\,k}^2} exp\left(-\frac{|\boldsymbol{x}|^2}{\sigma_{0\,k}^2}\right) \tag{6}$$

The vortex particles movement is governed by the vorticity transport equation, which is obtained by taking the curl of Eq. (2) and combining it with Eq. (1) (Batchelor, 2000):

$$\frac{\partial \bar{\omega}}{\partial t} + (\bar{\boldsymbol{u}} \cdot \nabla)\bar{\omega} = \frac{1}{Re_c}\nabla^2 \bar{\omega} \tag{7}$$

Where Re_c is the local Reynolds number modified by the local eddy viscosity coefficient, such as (Alcântara Pereira et al., 2003):

$$Re_{c_i}(t) = \frac{U^* D^*}{\nu + \nu_{t_i}(t)} \tag{8}$$

According to the viscous splitting algorithm, proposed by Chorin (1973), in the same simulation time increment, Δt^*, the advective and diffusive terms of the vorticity transport equation (Eq. 7) can be considered separately:

$$\frac{D\bar{\omega}}{Dt} = \frac{\partial \bar{\omega}}{\partial t} + (\bar{\boldsymbol{u}} \cdot \nabla)\bar{\omega} = 0 \tag{9}$$

$$\frac{\partial \bar{\omega}}{\partial t} = \frac{1}{Re_c} \nabla^2 \bar{\omega} \tag{10}$$

In this way, the discrete vortex displacement governed by Eq. (7) can be numeric calculated by solving Eq. (9) and Eq. (10) in each simulation time increment. The Eq (9) is solved by integrating each vortex blob path equation, and using an explicit Euler scheme, in the following form (Ferziger et al., 2020):

$$\boldsymbol{x_k}(t + \Delta t) = \boldsymbol{x_k}(t) + \bar{\boldsymbol{u}}(\boldsymbol{x_k}, t).\Delta t, \; k = 1, NV \tag{11}$$

Where the $\bar{\boldsymbol{u}}(\boldsymbol{x_k})$ is the velocity filtered field computed at position occupied by k−th vortex blob according to the Biot–Savart law (vortex–vortex interaction), panel method (vortex–panel interaction) and free stream velocity (vortex–mainstream interaction) contributions; for more details about these three contributions, see (1991).

The diffusive displacement of each vortex blob governed by Eq. 10 is solved using to the random walk method in the following form (Chorin, 1973):

$$\varsigma_k(t) = \sqrt{\frac{4\Delta t}{Re_c} ln\left(\frac{1}{P}\right)} \left[\cos(2\pi Q)_x + \sin(2\pi Q)_y\right] \tag{12}$$

Where P and Q are random numbers generated in the range: 0 < P < 1 and 0 < Q < 1 and the local Reynolds term, Re_c, presence indicates the turbulence computation. To compute the term Re_c such as described by Eq. (8) the local eddy viscosity coefficient, ν_t, needs to be evaluated. According to Alcântara Pereira et al. (2003), ν_t can be calculated by Eq. 4 with the characteristic length scale Δ^{+*} being the vortex bubbles radius, σ_0, and the local second-order velocity structure function obtained by:

$$\bar{F}_{2_k} = \frac{1}{N} \sum_{j=1}^{N} \left\| \bar{\boldsymbol{u}}(x_k) - \bar{\boldsymbol{u}}(x_k + r_j) \right\|_j^2 \left(\frac{\sigma_{0_k}}{r_j}\right)^{2/3} \tag{13}$$

After the new vortices positions were determined through Eq. (11) e Eq. (12) the actualized vorticity field is calculated by Eq. (6). The pressure field is calculated from the velocity field by the formulation developed by Shintani & Akamatsu (1994) and described in Bimbato et al. (2020) and Oliveira et al. (2020).

2.3. The Roughness Model

According to Bimbato et al. (2019) the roughness effect can be simulated in the two-dimension Lagrangian vortex method by adapting the vortices generation algorithm stage. At the vortex's generation, an injection of momentum in the flow boundary layer due to the roughness surface effects is calculated through a modified second-order velocity function, Eq (14), and numerically simulated by a vortex radius adjustment, Eq (15):

$$\bar{F}_{2_i}(\mathrm{t}) = \frac{1}{NR} \sum_{w=1}^{NR} \|\bar{\boldsymbol{u}}(x_i, t) - \bar{\boldsymbol{u}}(x_i + b, t)\|_w^2 \, (1 + \varepsilon) \tag{14}$$

$$\sigma_{0c_k}(t) = 1.41421 \sqrt{\frac{\Delta t}{Re}(1 + \frac{\nu_{t_i}(t)}{\nu})} \tag{15}$$

The $\bar{F}_{2_i}$ function is evaluated in the vicinity of the shedding point of the i-th panel adopting a semicircle, with radius $\|b\| = 2\varepsilon - \sigma_0$, and centered on i-th shedding point ($\varepsilon = \varepsilon^*/D^*$ is the mean relative surface roughness), Fig. 2. The local eddy viscosity coefficient ν_t is calculated by Eq. (4) considering the $\bar{F}_{2_i}$ function given by Eq. (14). When the roughness effects are simulated, each k-th vortex is generated with radius σ_{0c_k} instead of the σ_0 radius applied for all vortices in the smooth case (Bimbato et al., 2020).

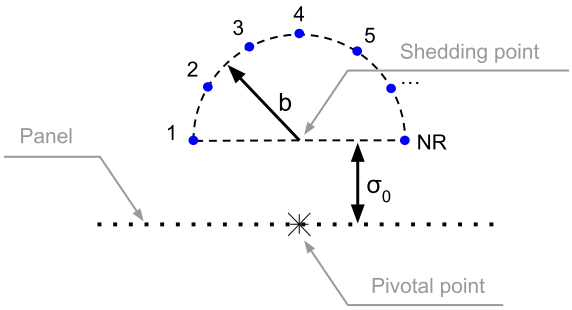

Figure 2. Position of the NR points used to calculate the modified second-order velocity function

2.4. The flat panels with vortex distribution of linear density

The body surface is discretized by flat panels over which singularities are distributed. The singularities intensities are calculated to annulate the normal velocity in the panel's pivotal points. The source is the type of singularity that, from the origin point, induces normal flow, whereas the vortex type induces a circular flow around the origin point. When singularities are distributed over the panel, the velocity induced by each panel depends on the singularity type, the distribution function ($f(x)$ Fig. 3a), geometric parameters (Fig. 3b), and the singularity strength ($\sigma(x)$ to a source distribution and $\gamma(x)$ to a vortex distribution).

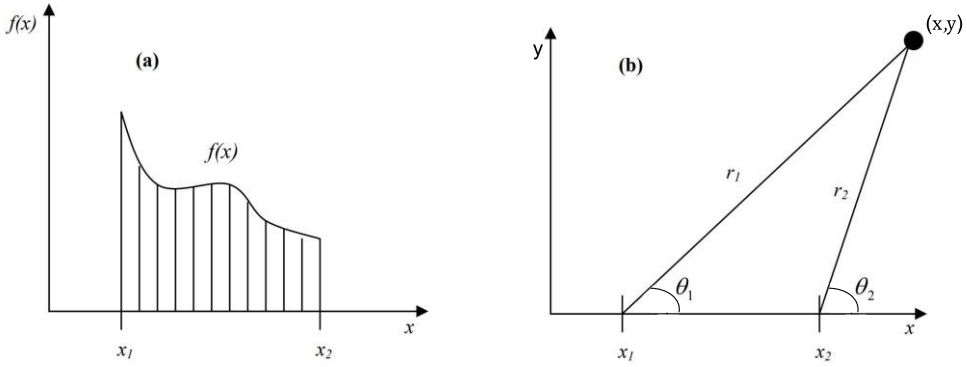

Figure 3. (a) Singularity distribution over a flat panel, (b) Point (x,y) position orientation from a flat panel

The velocity components x and y induced by a constant-density source distributed over a flat panel at the point $P(x, y)$ are given by Eq. (16) and Eq. (17), respectively. Eq. (18) and Eq. (19) are the induced velocity components at the same point $P(x, y)$ by a linear-density vortex distributed over a flat panel (Katz & Plotkin, 2001):

$$u_{Source} = \frac{\sigma}{2\pi} \ln \cdot \frac{r_1}{r_2} \tag{16}$$

$$v_{Source} = \frac{\sigma}{2\pi} (\theta_2 - \theta_1) \tag{17}$$

$$u_{Vortex} = \frac{\gamma_1}{2\pi(x_2 - x_1)} \left[(x_2 - x)(\theta_2 - \theta_1) - y \ln \frac{r_2}{r_1} \right] + \frac{\gamma_2}{2\pi(x_2 - x_1)} \left[x(\theta_2 - \theta_1) + y \ln \frac{r_2}{r_1} \right] \tag{18}$$

$$v_{Vortex} = \frac{\gamma_1}{2\pi(x_2 - x_1)} \left[(x_2 - x) \ln \frac{r_2}{r_1} - x_2 + y(\theta_2 - \theta_1) \right] + \frac{\gamma_2}{2\pi(x_2 - x_1)} \left[(x_2 - x_1) - y(\theta_2 - \theta_1) + x \ln \frac{r_2}{r_1} \right] \tag{19}$$

Where $\sigma(x)$ is the strength of the constant-density source distribution and γ_1 e γ_2 are the strengths of the vortex distribution at the panel extreme points x_1 and x_2, respectively; $r_s = \sqrt{(x-x_s)^2 + (y-y_s)^2}$ and $\theta_s = tan^{-1}[(y-y_s)/(x-x_s)]$ with $s = 1\ and\ 2$.

In the present work, the singularities type distributed over the panels is the linear-density vortex distribution, thus the velocity induced by each panel, which is a parcel of the advection velocity $\bar{\boldsymbol{u}}$ in Eq. (11), is calculated by Eq. (18) and Eq. (19), instead of Eq. (16) and Eq. (17), which are employed in the roughness model developed by Bimbato et al. (2019) and used in many others works (Alcântara Pereira et al., 2020; Bimbato et al., 2020; Moraes & Alcântara Pereira, 2021; Oliveira et al., 2020).

Besides the modification in the velocity-induced equations, the change of singularities, from source to vortex type, makes the generation vortex stage numerically simpler. The new vortices have intensities calculated to ensure the non-slip condition at the panels' pivotal point. The new k-th vortex intensity (Γ_k) is directly determined by the panel's vortex distribution strength (γ_1 e γ_2) and the panel length (Δs), as follows (Lewis, 1991):

$$\Gamma_k = \left[\frac{(\gamma_1+\gamma_2)}{2}\right]\Delta s \tag{20}$$

3. Results and Discussion

In this section, the numerical simulation of the two-dimensional, incompressible, unsteady flow, at $Re = 1 \times 10^5$, past around a circular cylinder is presented. In all simulations, the number of flat panels used to discretize the body surface is $m = 300$, the incremental time step is $\Delta t = 0.05$ and $NR = 21$ (Fig. 2), the same values used by Bimbato et al. (2019). As previously presented by Oliveira et al. (2020), all numerical simulations run until dimensionless time of $t = 75$, and the mean coefficient values (pressure distribution, drag and lift coefficients) are computed between $37.5 \leq t \leq 75.0$, when the saturation state of the numerical simulations is attained. In all simulations, the linear-density vortex distribution is the type of singularity used in the panel method.

For the case of turbulent flow past a smooth cylinder, the time histories of the drag and lift coefficients are shown in Fig. 4 (a), and the pressure coefficient (C_p) distribution over the cylinder surface is shown in Fig. 4 (b). The values for the mean drag coefficient, $\overline{C_D} = 1.231$, shows good agreement with experimental results of Blevins (1984), $\overline{C_D} = 1.200$, and numerical results using source distribution over the panels obtained by Bimbato et al. (2020), $\overline{C_D} = 1.223$. As shown in Fig 4(b), the time-averaged C_p distribution presented the same behavior registered experimentally by Blevins (1984).

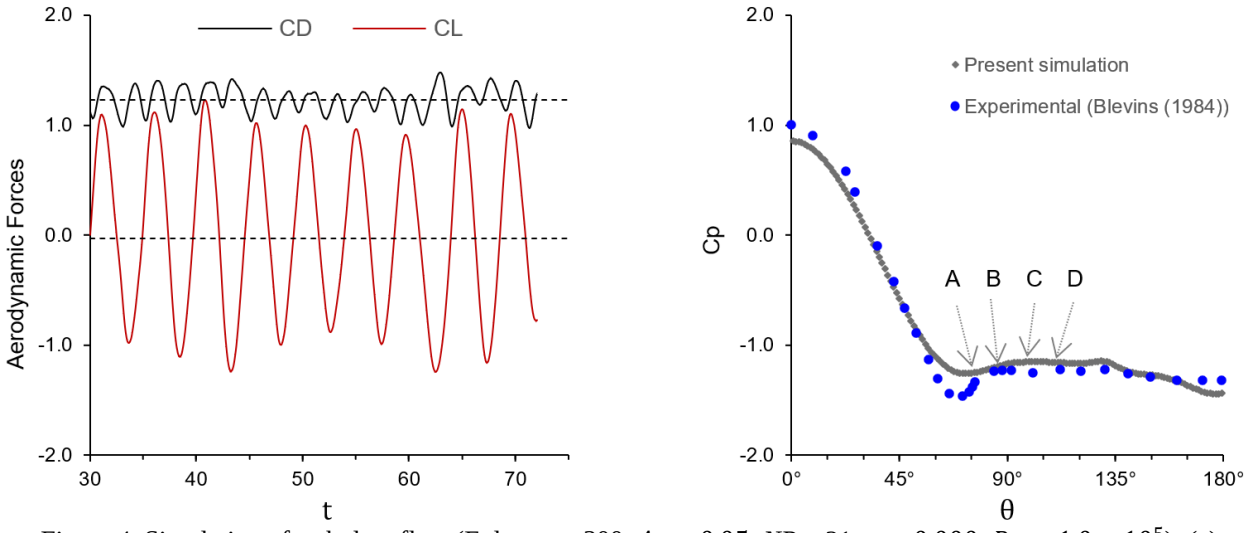

Figure 4. Simulation of turbulent flow (Euler; m = 300; $\Delta t = 0.05$, NR = 21; $\varepsilon = 0.000$; $Re = 1.0 \times 10^5$): (a) Temporal history for drag (C_D) and lift (C_L) coefficients, (b) Time-averaged pressure distribution around the circular cylinder surface.

The expected oscillatory behavior of the vortex wake can be observed by the oscillation of the C_D an C_L in Fig. 4 (a). The vortices structures in melting and dilution form an oscillatory wake, which can be observed, qualitatively, by

the instantaneous vortex blob distributions in Fig. 5. The vortex structure shedding frequency can be measured through the Strouhal number (*St*). For the turbulent flow past a smooth cylinder, the simulation registered $St = 0.194$, which is in very good agreement with experimental results of Blevins (1984), $St = 0.194$.

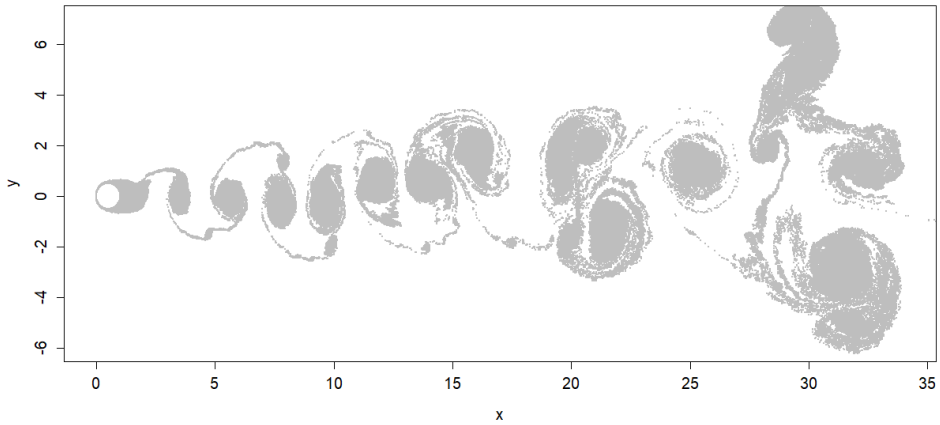

Figure 5. Vortices positions at $t = 45$ (Euler; m = 300; $\Delta t = 0.05$, NR = 21; $\varepsilon = 0.000$; $Re = 1.0 \times 10^5$).

According to data presented in Fig. 4, the simulation with linear-density vortex distribution was able to simulate the main characteristics of a turbulent flow around a hydraulic smooth bluff body at high Reynolds numbers. The drag coefficient $\overline{C_D} = 1.231$ is close to the value of $\overline{C_D} = 1.223$ find numerically by Bimbato et al. (2020) using source distributions. The same proximity with the Blevins (1984) experimental results obtained by Bimbato et al. (2020) was observed in the present simulation, Fig. 4(b).

As discussed in Section 1, the surface roughness effects modify the vortex wake dynamic, and as presented in Section 2.3, the roughness model rely on the injection of momentum in the boundary layer to simulate theses effects. Thus, the main characteristics that describe the vortex wake and the boundary layer behavior are following discussed, starting with the smooth cylinder and, then, investigating the flow modification caused by the turbulence consideration and the roughness simulation.

The vortex structures formation begins at the boundary layer separation point, measured by its angular position, θ_{sep}, and evolves over the recirculation region length. The fluid loads oscillatory behavior depends on θ_{sep}, the L_{rec} value, and the value of the base pressure coefficient (C_{p_b}). The θ_{sep} is determined by the angular position of the first pivotal point upstream in which an adverse flow start near the solid surface; at this point the C_p gradient is zero. The separation point can be verified at the angular position $\theta_{sep} = 79.8^{\circ}$, where C_p gradient is zero (Fig.4). The adverse flow can be verified by the boundary layer velocity profile at the identified pivotal points shown in Fig. 6 (b). The pivotal points identified at Fig. 6(a) are highlighted in Fig. 4(b), and the base pressure coefficient is measured at point *F* having the value $C_{p_b} = -1.438$.

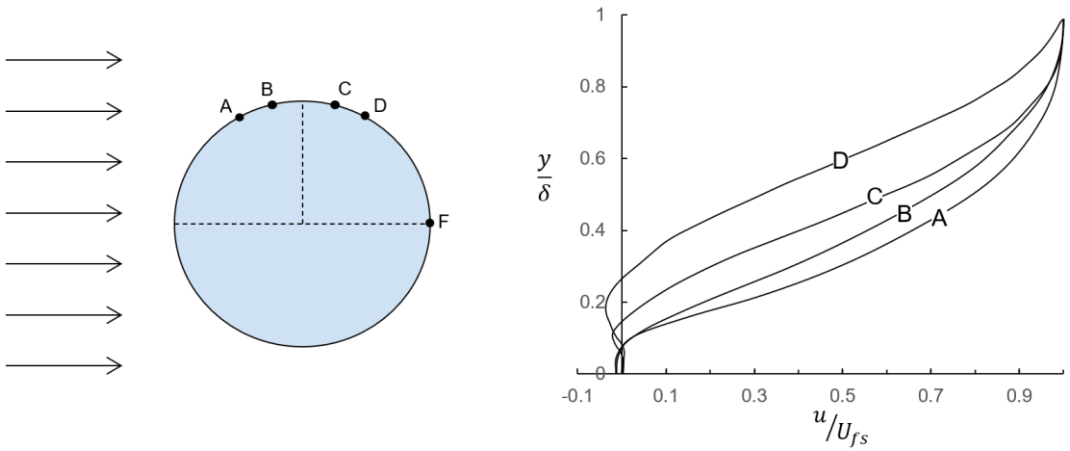

Figure 6. Boundary layer characteristics: (a) Simulation scheme with the points analyzed (b) boundary layer velocity profile at locations on the cylinder (Euler; m = 300; $\Delta t = 0.05$, NR = 21; $\varepsilon = 0.000$; $Re = 1.0 \times 10^5$).

In Tab. 1, the results previously discussed, from the simulations of the turbulent flow past around a smooth cylinder, are compared with the results from simulations considering a laminar flow past over a smooth cylinder and the results considering the turbulent flow with roughness effect.

Table 1. Summary for the simulation results

Case	ε	$\overline{C_D}$	C_L	St	$-C_{p_b}$	θ_{sep}
Turbulent	0.000	1.231	-0.006	0.194	1.438	79.8
Laminar	0.000	1.310	0.0024	0.190	1.551	74.0
Turbulent	0.007	1.191	-0.0032	0.209	1.418	85.0

In Tab. 1, from the laminar flow case to the turbulent case, momentum is injected into the boundary layer due to turbulence consideration. The momentum injection contributes to flow to support the adverse pressure gradient present in the boundary layer, changing the vortex wake and boundary layer characteristics. The turbulence consideration delayed the separation point in 5.8°, in relation to the laminar simulations, and the base pressure coefficient increased 7.3%, together with a slight change of 2.1% in the Strouhal number. The delay in the separation point causes the expected drag coefficient reduction, as discussed by Williamson (1996).

The roughness model with the linear-density vortex singularity type was able to anticipate to lower Reynolds number ($Re = 1 \times 10^5$), at subcritical regime, phenomena expected to happen at higher Reynolds numbers, at critical regime. The augmentation of the Strouhal number ($\Delta St = +7.7\%$), with the increasing of base coefficient ($\Delta C_{p_b} = +1.4\%$) and the delay of the separation point ($\Delta\theta_{sep} = +5.2^{\circ}$) are compatible with the experimental work of Achenbach & Heinecke (1981) and the numerical work of Bimbato et al. (2020).

The main consequence of the flow changing due to the roughness effects, as described in Section 1, is the modification of the aerodynamic loads. At the present simulations, de drag coefficient for the same turbulent flow Reynolds numbers $Re = 1.0 \times 10^5$ decreased from $\overline{C_D} = 1.231$ to $\overline{C_D} = 1.191$ (-3,25%), for a rough surface of $\varepsilon = 0.007$. For the same rough dimension and *Re* flow number, using source distributions, Bimbato et al. (2020) found a decrease from $\overline{C_D} = 1.223$ to $\overline{C_D} = 1.071$ (-12.43%).

In Fig. 7 the vortex wake downstream the circular cylinder at $t = 45$ is shown for the turbulent flow past the rough circular cylinder. The instantaneous vortices positions indicate that the vortical structures for the rough cylinder are narrower than the structures for the smooth cylinder (Fig. 5), which is in accordance with what is expected from critical flow regimes, as a consequence of the phenomena's anticipation provoked by roughness, as previously discussed.

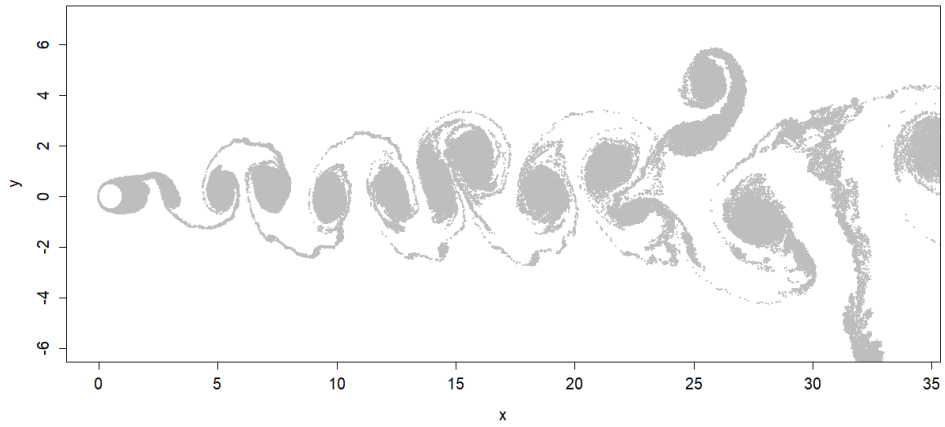

Figure 7. Vortices positions at $t = 45$ (Euler; $\varepsilon = 0.007$; $m = 300$; $\Delta t = 0.05, NR = 21$; $Re = 1.0 \times 10^5$)

4. CONCLUSION

The present work implements an adaption to the Lagrangian vortex method using a two-dimensional roughness model developed by Bimbato et al. (2019). In the simulations presented here, the panel method with linear-density vortex distribution was used in order to verify the possibility of applying the roughness model developed by Bimbato et al. (2019) to study the flow around non-symmetrical bodies, which are characterized by lift force generation. The modified algorithm was able to capture the roughness effects in the vortex wake behavior, correctly registering the changes in aerodynamics loads when rough bodies was simulated. Flow at subcritical Reynolds number past smooth circular cylinder was simulated and the results were compared to data from the simulation of the same flow of the rough cylinder. A displacement at the separation point, an augmentation in Strouhal number, and a drop in drag coefficient expect to happen at critical Reynolds, were obtained at the subcritical Reynolds number as a result of the roughness surface action.

Although the adapted algorithm was able to capture the roughness influence in anticipating critical flow patterns to physical subcritical flow, the falling in drag coefficient is smaller than the numerical values of Bimbato et al. (2020) work with source distribution and the experimental values of Achenbach & Heinecke (1981). Additional analysis will have to be carried out to verify if the time and space discretization besides the roughness model parameters have any influence on this issue.

Finally, the authors intend to apply the adapted code to study practical engineering situations in flow past slender bodies, such as the stall delay and the viscous drag coefficient increase due to roughness effects.

5. ACKNOWLEDGEMENTS

The authors would like to acknowledge São Paulo Research Foundation (FAPESP), grant 2022/03630-4, and Coordenação de Aperfeiçoamento de Pessoal de Nível Superior (CAPES/Brasil) - Finance-Code-001.

6. REFERENCES

Achenbach, E., & Heinecke, E. (1981). On vortex shedding from smooth and rough cylinders in the range of Reynolds numbers 6×10 3 to 5×10 6. *Journal of Fluid Mechanics*, *109*, 239–251.

Adams, T., Grant, C., & Watson, H. (2012). A Simple Algorithm to Relate Measured Surface Roughness to Equivalent Sand-grain Roughness. *International Journal of Mechanical Engineering and Mechatronics*.

Alcântara Pereira, L. A., de Oliveira, M. A., de Moraes, P. G., & Bimbato, A. M. (2020). Numerical experiments of the flow around a bluff body with and without roughness model near a moving wall. *Journal of the Brazilian Society of Mechanical Sciences and Engineering*, *42*(3), 129.

Alcântara Pereira, L. A., Hirata, M. H., & Silveira Neto, A. (2003). Vortex method with turbulence sub-grid scale modeling. *Journal of the Brazilian Society of Mechanical Sciences and Engineering*, *25*, 140–146.

Batchelor, G. K. (2000). *An Introduction to Fluid Dynamics*. Cambridge University Press.

Bimbato, A. M., Alcântara Pereira, L. A., & Hirata, M. H. (2019). Development of a new Lagrangian vortex method for evaluating effects of surfaces roughness. *European Journal of Mechanics - B/Fluids*, *74*, 291–301.

Bimbato, A. M., Alcântara Pereira, L. A., & Hirata, M. H. (2020). Study of Surface Roughness Effect on a Bluff Body—The Formation of Asymmetric Separation Bubbles. *Energies*, *13*(22), 6094.

Blevins, R. ~D. (1984). *Applied fluid dynamics handbook*.

Chakroun, W., Al-Mesri, I., & Al-Fahad, S. (2004). Effect of Surface Roughness on the Aerodynamic Characteristics of a Symmetrical Airfoil. *Wind Engineering*, *28*(5), 547–564.

Chen, W., Wang, S., Shi, X., Rheem, C.-K., Lin, Y., & Liu, E. (2022). Numerical simulation of surface roughness effects on the vortex-induced vibration of a circular cylinder at a subcritical Reynolds number. *International Journal of Naval Architecture and Ocean Engineering*, *14*, 100430.

Chorin, A. J. (1973). Numerical study of slightly viscous flow. *Journal of Fluid Mechanics*, *57*(4), 785–796.

Chung, D., Hutchins, N., Schultz, M. P., & Flack, K. A. (2021). Predicting the Drag of Rough Surfaces. *Annual Review of Fluid Mechanics*, *53*(1), 439–471

Dalili, N., Edrisy, A., & Carriveau, R. (2009). A review of surface engineering issues critical to wind turbine performance. *Renewable and Sustainable Energy Reviews*, *13*(2), 428–438.

Ferziger, J. H., Perić, M., & Street, R. L. (2020). *Computational Methods for Fluid Dynamics*. Springer International Publishing.

Fiore, G., & Selig, M. S. (2015). Simulation of Damage for Wind Turbine Blades Due to Airborne Particles. *Wind Engineering*, *39*(4), 399–418.

Gao, Y., Zong, Z., Zou, L., Takagi, S., & Jiang, Z. (2018). Numerical simulation of vortex-induced vibration of a circular cylinder with different surface roughnesses. *Marine Structures*, *57*, 165–179.

Güven, O., Farell, C., & Patel, V. C. (1980). Surface-roughness effects on the mean flow past circular cylinders. *Journal of Fluid Mechanics*, *98*(4), 673–701.

Han, X., Tang, Y., Meng, Z., Fu, F., Qiu, A., Gu, J., & Wu, J. (2021). Surface roughness effect on cylinder vortex-induced vibration at moderate Re regimes. *Ocean Engineering*, *224*, 108690.

Henderson, R. D. (1995). Details of the drag curve near the onset of vortex shedding. *Physics of Fluids*, *7*(9), 2102–2104.

Katz, J., & Plotkin, A. (2001). *Low-Speed Aerodynamics*. Cambridge University Press.

Kodancha, P., & Salunkhe, P. B. (2021). Influence of Blade Tip Surface Roughness on the Performance of a Single-Stage Axial Flow Compressor. *Journal of Fluids Engineering*, *143*(6).

Lesieur, M., & Metais, O. (1996). New Trends in Large-Eddy Simulations of Turbulence. *Annual Review of Fluid Mechanics*, *28*(1), 45–82.

Lewis, R. I. (1991). *Vortex Element Methods for Fluid Dynamic Analysis of Engineering Systems*. Cambridge University Press.

Liang, C., & Papadakis, G. (2007). Large eddy simulation of pulsating flow over a circular cylinder at subcritical Reynolds number. *Computers & Fluids*, *36*(2), 299–312.

Moraes, P. G. de, & Alcântara Pereira, L. A. (2021). Surface Roughness Effects on Flows Past Two Circular Cylinders in Tandem Arrangement at Co-Shedding Regime. *Energies*, *14*(24), 8237.

Norberg, C. (1994). An experimental investigation of the flow around a circular cylinder: influence of aspect ratio. *Journal of Fluid Mechanics*, *258*, 287–316.

Oliveira, M. A. de, Moraes, P. G. de, Andrade, C. L. de, Bimbato, A. M., & Alcântara Pereira, L. A. (2020). Control and Suppression of Vortex Shedding from a Slightly Rough Circular Cylinder by a Discrete Vortex Method. *Energies*, *13*(17), 4481.

Pour, M. (2018). Determining surface roughness of machining process types using a hybrid algorithm based on time series analysis and wavelet transform. *The International Journal of Advanced Manufacturing Technology*

Roshko, A. (1993). Perspectives on bluff body aerodynamics. *Journal of Wind Engineering and Industrial Aerodynamics*, *49*(1–3), 79–100.

Schewe, G. (1983). On the force fluctuations acting on a circular cylinder in crossflow from subcritical up to transcritical Reynolds numbers. *Journal of Fluid Mechanics*, *133*, 265–285.

Shintani, M., & Akamatsu, T. (1994). Investigation of Two Dimensional Discrete Vortex Method with Viscous Diffusion Model. *Computational Fluid Dynamics Journal*, *3*(2), 237–254.

Slaouti, A., & Gerrard, J. H. (1981). An experimental investigation of the end effects on the wake of a circular cylinder towed through water at low Reynolds numbers. *Journal of Fluid Mechanics*, *112*(1), 297.

Smagorinsky, J. (1963). GENERAL CIRCULATION EXPERIMENTS WITH THE PRIMITIVE EQUATIONS. *Monthly Weather Review*, *91*(3), 99–164.

Toba, D., Fukudome, K., Mamori, H., Fukushima, N., & Yamamoto, M. (2020). Proposal of Novel Icing Simulation Using a Hybrid Grid- and Particle-Based Method. *Journal of Mechanics*, *36*(5), 699–706.

Unal, M. F., & Rockwell, D. (1988). On vortex formation from a cylinder. Part 1. The initial instability. *Journal of Fluid Mechanics*, *190*, 491–512.

van Hinsberg, N. P. (2015). The Reynolds number dependency of the steady and unsteady loading on a slightly rough circular cylinder: From subcritical up to high transcritical flow state. *Journal of Fluids and Structures*, *55*, 526–539.

Wang, M. Y., Hashmi, S. A., Sun, Z. X., Guo, D. L., Vita, G., Yang, G. W., & Hemida, H. (2021). Effect of surface roughness on the aerodynamics of a high-speed train subjected to crosswinds. *Acta Mechanica Sinica*, *37*(7), 1090–1103.

Williamson, C. H. K. (1996). Vortex Dynamics in the Cylinder Wake. *Annual Review of Fluid Mechanics*, *28*(1), 477–539.

Zdravkovich, M. M., & Bearman, P. W. (1998). Flow Around Circular Cylinders—Volume 1: Fundamentals. *Journal of Fluids Engineering*, *120*(1), 216–216.

Zhang, B., Mao, X., Wu, X., & Liu, B. (2021). Effects of Tip Leakage Flow on the Aerodynamic Performance and Stability of an Axial-Flow Transonic Compressor Stage. *Energies*, *14*(14), 4168

7. RESPONSIBILITY NOTICE

The authors are the only responsible for the printed material included in this paper.